Chapter 21
Model Calibration and Uncertainty of A600 Wind Turbine Blades

Anders T. Johansson, Andreas Linderholt, and Thomas Abrahamsson

Abstract Recently, a lot of work has been done on modeling, testing and calibrating Ampair 600 W wind turbine blades, owing to the use of that turbine as a test bed structure for the Dynamic Substructuring Focus Group within the Society of Experimental Mechanics. In Sweden alone, more than 20 blades have been tested for dynamical properties, geometrical differences and material properties as was presented in several papers at IMAC XXXI. The quantity of blades, originating from different manufacturing batches, makes them ideal for investigations of component variability.

In this paper, measurement variability predominantly stemming from the difference between individual blades is propagated backwards to model parameters, using model calibration techniques, in an effort to quantify their uncertainties. The coupling between spread in structural properties such as mass, center of gravity and blade twist angles and spread in the resulting blade dynamics is shown.

Keywords Model calibration • A600 wind turbine blade • Manufacturing spread • Twisting angle • Vibrational tests

21.1 Introduction

A production sequence will always be precise only within given tolerances, causing a spread between individuals within a produced population. This spread stems from a variety of sources, such as material spread, production process variability and finite precision in the assembly of components. In order to make qualified predictions of components from a production sequence, quantification of such variations, in terms of inputs to the model used to make the predictions, is essential [1]. Here, the hypothesis is that such variations can be captured using model calibration setting out from vibrational data stemming from tests made on several individuals. Frequently, such backward propagations of uncertainty parameters are made by application of Monte Carlo methods by assuming or fitting a probability distribution to the output data, either in a frequentist or a Bayesian setting [2, 3]. In this paper, the model will instead be calibrated to each individual in a family of 20 blades. Our motivation for using such a time-consuming approach is that it does not require any assumptions on the output data distribution. Furthermore, it enables high quality validation of the spread at parameter level through dedicated testing. Since the method does not rely on any assumptions on the distribution of data, the results may also come to good use in evaluating stochastic model updating techniques.

The SEM Substructuring Focus Group has chosen the Ampair 600 W wind turbine, seen in Fig. 21.1, as a benchmark test bed for studies of substructuring. Since its introduction at IMAC XXX [4], such studies have been carried out by several institutes in a number of countries, e.g. [5–7]. This study will focus on the blades of said wind turbine.

Twenty A600 wind turbine blades are evaluated in this study. The blades are grouped in the sets of three in which they were delivered by the wind turbine manufacturer [8]. These are here classified by the capital letters A–G. The following

A.T. Johansson (✉) • T. Abrahamsson
Department of Applied Mechanics, Chalmers University of Technology, 41296 Göteborg, Sweden
e-mail: anders.t.johansson@chalmers.se

A. Linderholt
Department of Mechanical Engineering, Linnaeus University, 35195 Växjö, Sweden

H.S. Atamturktur et al. (eds.), *Model Validation and Uncertainty Quantification, Volume 3: Proceedings of the 32nd IMAC, A Conference and Exposition on Structural Dynamics, 2014*, Conference Proceedings of the Society for Experimental Mechanics Series, DOI 10.1007/978-3-319-04552-8_21, © The Society for Experimental Mechanics, Inc. 2014

Fig. 21.1 The Ampair 600 W turbine (*Source*: http://www.ampair.com/)

serial numbers constitute the seven sets: A = {828, 852, 790}, B = {841, 722, 819}, C = {878, 877, 881}, D = {963, 962, 948}, E = {905, 912}, F = {893, 906, 907} and G = {888, 892, 895}. Set E contains only two blades since one blade was used in destructive testing.

21.2 Blade Dynamics Characterization

The blades were examined by vibrational testing to study the spread in blade dynamics and produce data for the subsequent model updating procedure. The blades in groups A–D were tested, by students at Chalmers University of Technology in Sweden [9], using shaker excitation at position 3 whereas the blades in E–G were tested, by students at Linnaeus University in Sweden [10], using hammer excitation at position 1. For the vibrational tests used in this paper, the blades are hung in flexible suspensions to mimic free-free support conditions. The 20 positions used for the actuators and sensors follows the measurement setup described in [11] and are also shown in Fig. 21.2. The measured eigenfrequency statistics for the first eight modes are given as box plots in Fig. 21.3. Note that the seventh mode is likely to be an edgewise bending mode (cf. [12]) which may not be identifiable from the measurements as all sensing and actuation takes place in the direction perpendicular to its main plane of motion, wherefore the results at the top part of the figure should be interpreted cautiously. Throughout this paper, the first six eigenmodes, i.e. the rigid body modes, are omitted and thus when referring to the first mode it is implied to be the first elastic mode. It is seen that groups E–G generally show lower mean frequency values than these of groups A–D. This may be explained by the statistical spread between batches. However, the difference in excitation methods cannot be excluded as a cause to the differences. ANOVA indicates that the probability of the null hypothesis that the first mode of each blade stems from the same population is less than 1 %. Furthermore, results in literature where impact hammer testing has been used also report significantly lower natural frequencies than those of blade A–D here [11].

21.3 Model Calibration

The hypothesis is that setting out from a nominal finite element model, based on engineering skills and experience, and having a good parameterization, calibrations of the physical parameters will enable the model to closely resemble the output of any of the blades. If successful, the model calibration process will hence capture the statistics of the parameters.

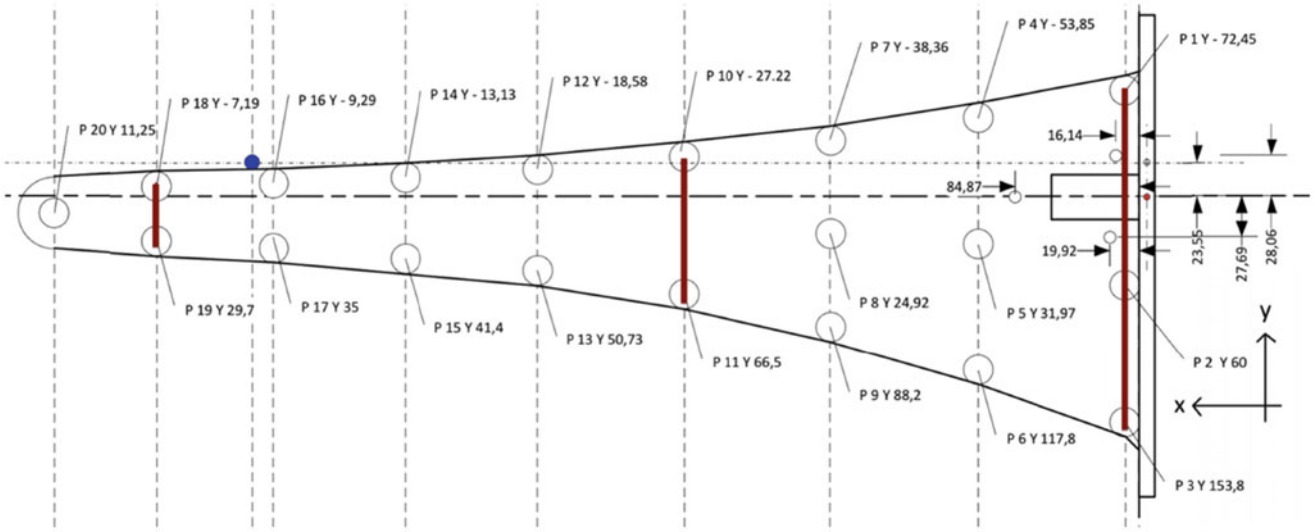

Fig. 21.2 The *circles* symbolize the positions used for actuators and sensors during vibrational tests. The *three thick solid lines* mark the locations at which the twist angles are measured

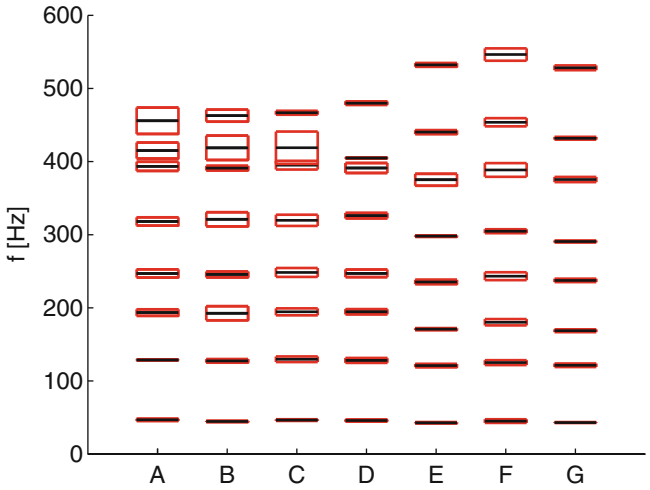

Fig. 21.3 Statistics for the eight first elastic eigenmodes. For each blade group (the columns), the mean value of the frequency for each mode is represented by a *black line*. Plus and minus one standard deviation, setting out from the mean values, are represented by a *red box* (color figure online)

21.3.1 FE-Modeling

The model used is a version of the calibrated model described in [12]. The outer geometry of the blade was provided by the substructuring focus group, from which an MSC NASTRAN FE-model was made using the pre- and postprocessor FEMAP. It consists of a laminate skin on an isotropic core. The material in the skin is glass fibers weave reinforced polypropylene, while the core consists of polypropylene only [12]. The skin, 2.8 mm thick, is modeled by four equal layers in a 0°–90°–0°–90° stack where each layer has the stiffness properties of the calibrated model in [12], i.e. $E_1 = 14.5$ GPa, $E_2 = 1.75$ GPa and the shear moduli $G_{12} = 0.9$ GPa in plane and $G_{1z} = G_{2z} = 0.72$ GPa out of plane. The equivalent orthotropic stiffness of the skin is 6.77 GPa for both fiber directions. The core modulus is $E = 1.67$ GPa and the corresponding Poisson's ratio is $\nu = 0.3$. The density of the core and the skin is chosen to match the weight of blade number 963 at 272 kg/m^3 and 818 kg/m^3, respectively, yielding a mass of 798.6 g (referring to [12] for a motivation of the low density of the skin). The skin is modeled using four-noded rectangular plate elements with a few triangular elements, and the core is modeled by four-noded tetrahedral elements. Additional verification studies as compared to those of [12] allowed a reduction in size, such that the model used in this study consists of 95,897 elements and 20,517 nodes.

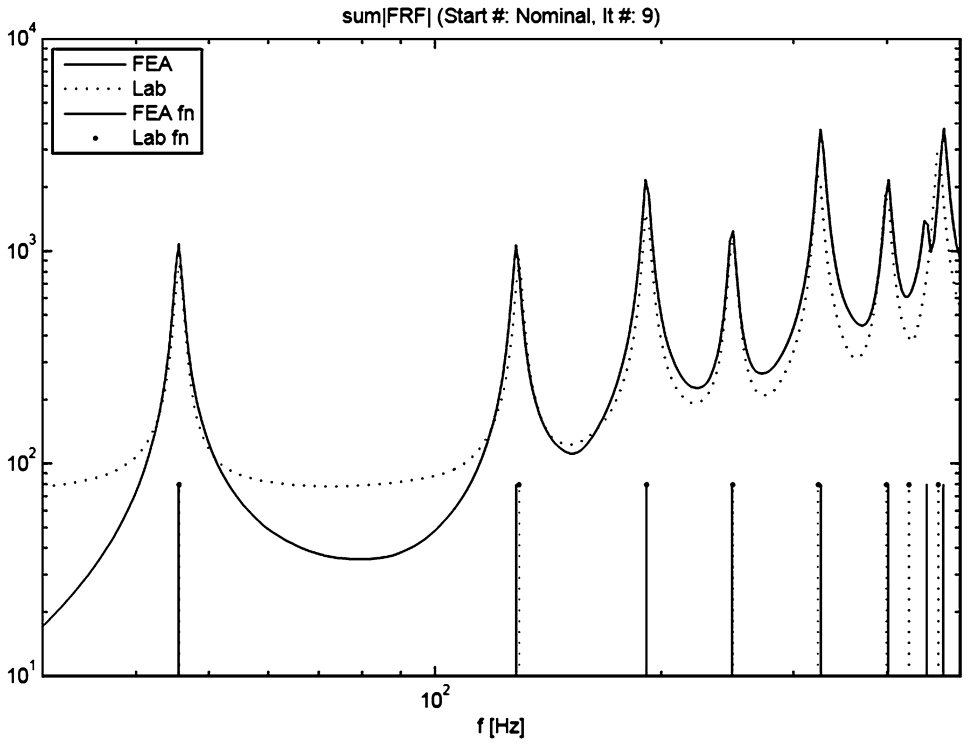

Fig. 21.4 Sum of the absolute value of Frequency Response Functions of model calibrated to data from Blade number 828. *Dotted line* is measured data. Eigenfrequencies are represented by *vertical lines*. Note that the seventh mode, an edgewise bending mode, is not visible in the data and has not been calibrated well. Whether the experimental model or the FE model is erroneous is unclear

21.3.2 Calibration Method

The calibration method used in this study uses a frequency band based deviation metric in conjunction with a damping equalization technique minimized by the Levenberg-Marquardt optimization method and utilizing multiple starting points from a Latin Hypercube sampling procedure to ensure global convergence [13–15]. The damping equalization technique requires the use of a test model, in this case identified using the system identification toolbox in Matlab and the function n4sid [16, 17]. The model matrices are linearized in the parameters about the nominal value numerically, thus the Jacobian used in the Levenberg-Marquardt method is easily computed. An open-source Matlab code known as *FEMcali* was used for the calibration [18].

The parameters used in the optimization are the three in-plane properties of the skin E_1, E_2 and G_{12} and the Young's modulus of the core E. The two out-of-plane shear moduli were left out of the calibration after a parameter identifiability analysis showing that they were not identifiable from the measured data. Furthermore, parameter bounds were used to ensure that the results remained physical. The upper bounds were never reached, but the lower bounds for E_2, G_{12} and E were 1.00 GPa, 0.40 GPa and 0.80 GPa, respectively. This is verified by the results in [12]. Ten different starting points were used for each blade in the calibration step.

21.3.3 Calibration Results

A typical output result for one of the blades is seen in Fig. 21.4, and the calibration results are presented in Table 21.1. All the runs converged in much the same way as presented in Fig. 21.4 for blade number 828—the identifiable modes were within a few percent error.

It is seen in Table 21.1 that the spread in material properties is quite high and that at least one parameter hits a bound for every blade, likely caused by an overparameterization of the model with respect to the calibration metric used. Furthermore, the most influential parameter, the fiber stiffness, is always higher for the blades measured with stinger excitation. In calculating the corresponding orthotropic stiffness parameters, the mean and standard deviation become $\mu = 5.9$ GPa and $\sigma = 0.57$ GPa, however, indicating a comparatively tighter band, which is in agreement with the perceived high quality of the calibration results.

Table 21.1 Calibration results

	A			B		
	828	852	790	841	722	819
E_1	11.2 GPa	14.2 GPa	13.3 GPa	13.9 GPa	12.4 GPa	12.8 GPa
E_2	1.00 GPa	1.00 GPa	1.00 GPa	1.00 GPa	1.00 GPa	1.00 GPa
G_{12}	0.50 GPa	1.24 GPa	1.32 GPa	1.28 GPa	1.28 GPa	0.77 GPa
E	1.95 GPa	0.80 GPa	0.87 GPa	0.84 GPa	1.07 GPa	1.39 GPa
		C			D	
	878	877	881	963	962	948
E_1	10.6 GPa	15.3 GPa	13.1 GPa	11.4 GPa	13.2 GPa	14.1 GPa
E_2	1.00 GPa	1.06 GPa	1.66 GPa	1.00 GPa	1.13 GPa	1.29 GPa
G_{12}	0.42 GPa	1.36 GPa	1.48 GPa	0.50 GPa	1.45 GPa	1.44 GPa
E	1.99 GPa	0.80 GPa	0.80 GPa	1.97 GPa	0.80 GPa	0.80 GPa
		E			F	
		905	912	893	906	907
E_1		7.57 GPa	8.13 GPa	7.90 GPa	7.31 GPa	10.38 GPa
E_2		5.90 GPa	3.50 GPa	5.20 GPa	4.94 GPa	1.97 GPa
G_{12}		0.40 GPa	0.40 GPa	0.40 GPa	0.40 GPa	0.40 GPa
E		1.57 GPa	1.63 GPa	1.74 GPa	1.72 GPa	1.83 GPa
		G				
	888	892	895		μ	σ
E_1	9.94 GPa	9.31 GPa	9.71 GPa		11.3 GPa	2.45 GPa
E_2	1.61 GPa	2.55 GPa	1.81 GPa		2.03 GPa	1.57 GPa
G_{12}	0.40 GPa	0.40 GPa	0.40 GPa		0.181 GPa	0.47 GPa
E	1.54 GPa	1.64 GPa	1.54 GPa		1.36 GPa	0.46 GPa

The grey marking indicates that a parameter has hit a bound

21.4 Validation

To validate the parameter values found by the model calibration, a number of tests were made to get reliable values of the actual properties of the blades.

21.4.1 Skin Material

The skin is a composite consisting of Polypropylene reinforced with woven glass fiber. Hence, it is expected that the material properties are dependent on the direction. A piece of the woven glass fiber material used for the blade shows that the fibers are woven in 2/2 twill style. Direction (1) is along the weft threads, expected to be the strongest direction, since the threads are pretty straight. Direction (2) is along the warp threads crossing the weft perpendicular and are going up and down around them, see Fig. 21.5.

A flat, rectangular sample of skin material was provided by the wind turbine manufacturer Ampair Energy Ltd. Nine specimens were cut out from the sample, see Fig. 21.6. While applying tensional forces to the specimens, the deformations are measured using two extensometers which enables handling possible bendings. Additionally, the applied force is recorded. The results of the tensile tests are given in Table 21.2.

21.4.2 Core Material

Compression tests of the foam material constituting the blade core are made. It is assumed, that the core is isotropic. A cube of the core material was provided by Ampair Energy Ltd. From this cube, two test specimens are machined, see Fig. 21.7. While compressing the core material specimens, the compression is measured by two extensometers which are arranged perpendicular to each other. The Young's moduli found from the compression tests of the core material are shown in Table 21.3.

The average value, for the Young's modulus, of 1.42 GPa corresponds to values given in literature. According to [19] typical values for the Young's modulus of Polypropylene are within the range from 1.3 to 1.8 GPa.

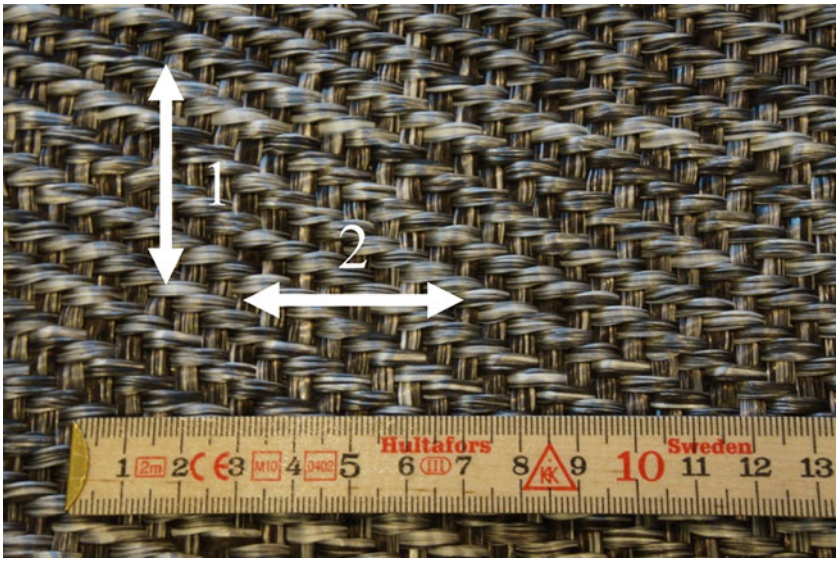

Fig. 21.5 The woven glass fiber material used in the blade skins

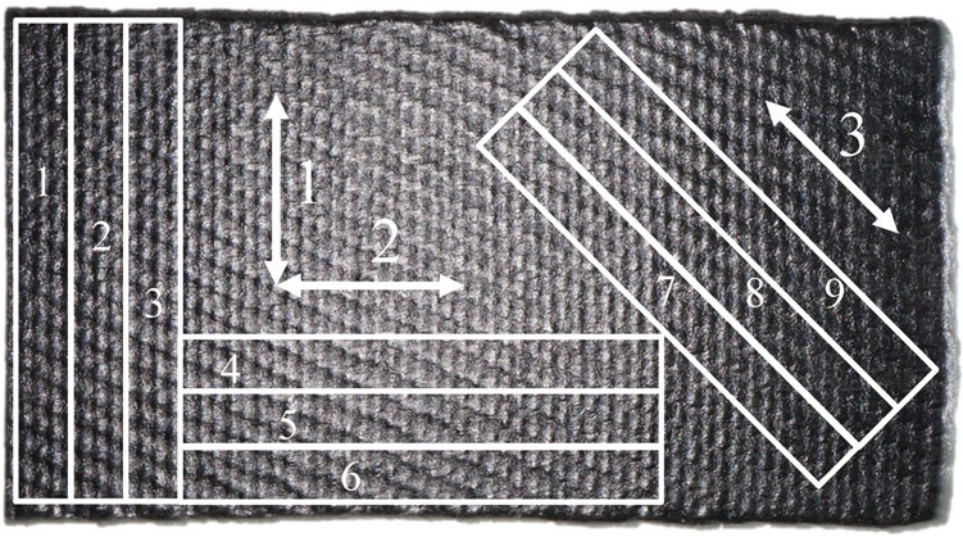

Fig. 21.6 Orientation of the specimens cut out from the sample plate. *Arrows* are showing the three directions of the test specimens (1–3: 0°, 4–5: 90°, 7–9: 45°)

Table 21.2 Test results for tensile tests

Specimen No.	Direction	Young's modulus (GPa)	Mean value Young's modulus (GPa)
1	1	11.91	11.85
2	1	11.87	
3	1	11.76	
4	2	9.66	10.17
5	2	10.00	
6	2	10.90	
7	3	2.36	2.30
8	3	2.17	
9	3	2.36	

Out of one of the blades, cylindrical disks were cut out and X-rayed. In Fig. 21.8, the core material is seen for two locations in the same blade. It is clear that the porosity of the core and thereby its effective Young's modulus has a severe variation (0.3 % versus 8 % volume porosity). That does not seem to be the case for the core material test specimen. That can be an explanation to the difference between the Young's modulus for the core that is found from calibration and that found from the compression tests.

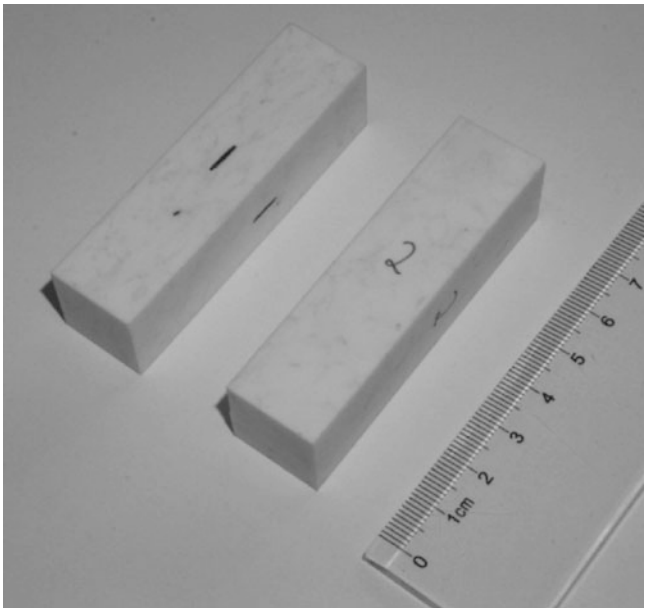

Fig. 21.7 Test specimens for the compression tests

Table 21.3 Results of the core-material compression tests

No.	Width (mm)	Thickness (mm)	Length (mm)	Area (mm)	Young's modulus (GPa)	Mean value Young's modulus (GPa)
1	19.05	19.05	72.22	362.9	1.43	1.42
2	19.06	19.06	72.24	363.3	1.41	

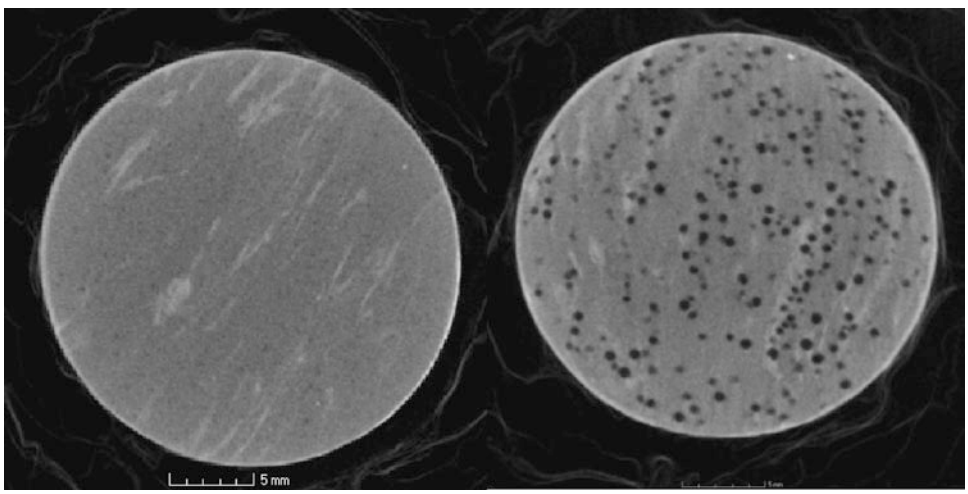

Fig. 21.8 Cross sections of two disks cut out from a blade, showing the core material

21.4.3 Blade Mass Properties

A Computer Tomography (CT) scan was made for two of the blades to study how they are built up. In the first blade a cylindrical insert having larger density than steel was found, see Fig. 21.9. The scanning of the other blade revealed two inserts at locations different from that of the first blade. It is reasonable to believe that the inserts are used for balancing. Weighting of the blades in the seven groups shows that the masses of blades within the same group are close whereas the differences between groups are much larger. The blades are delivered in packages of three to be assembled to one turbine. From [9] it is known, that the turbine blades are grouped in packages considering the weight but there is no evidence of further groupings related to dynamic properties. Here, the spread in center of gravity is studied to examine if also the center of gravity is used for the balancing and grouping the blades. A simple methodology where the blades were hanged in vertical lines traced by lasers is used to calculate the center of gravity (COG) of the blades, see Fig. 21.10. The ANOVA, Fig. 21.11, indicates that the blades have indeed been balanced together in groups (with a probability of null hypothesis well below one tenth of a percent for the x-direction).

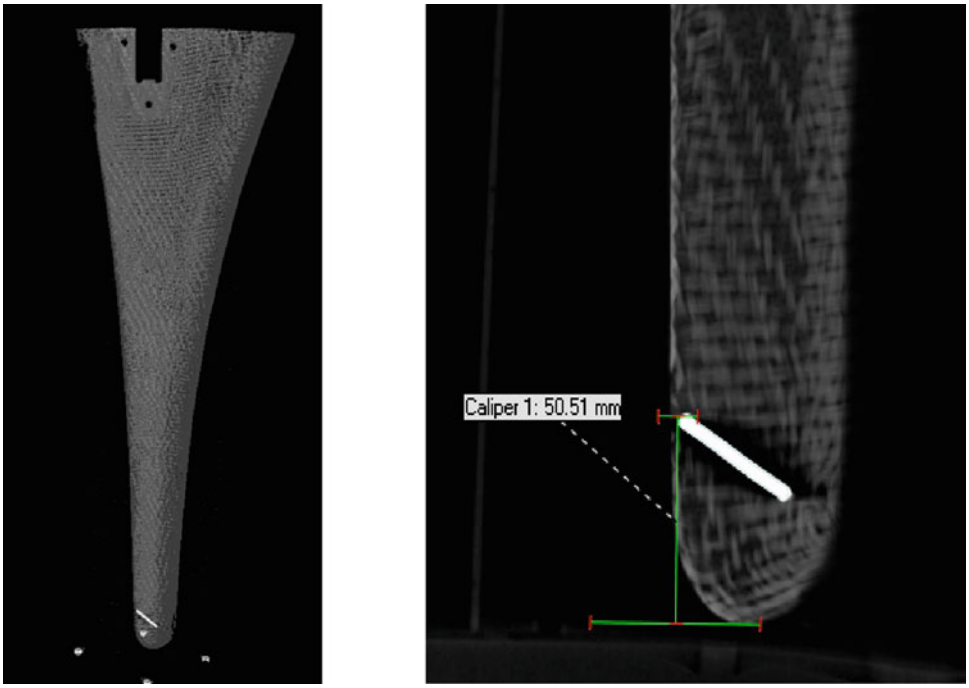

Fig. 21.9 The angle that the insert makes relative to the nearest blade edge is 124°. The length and volume were determined as 34.4 mm and 700 mm^3 and the distance from the tip vertically along the blade edge is 50.5 mm

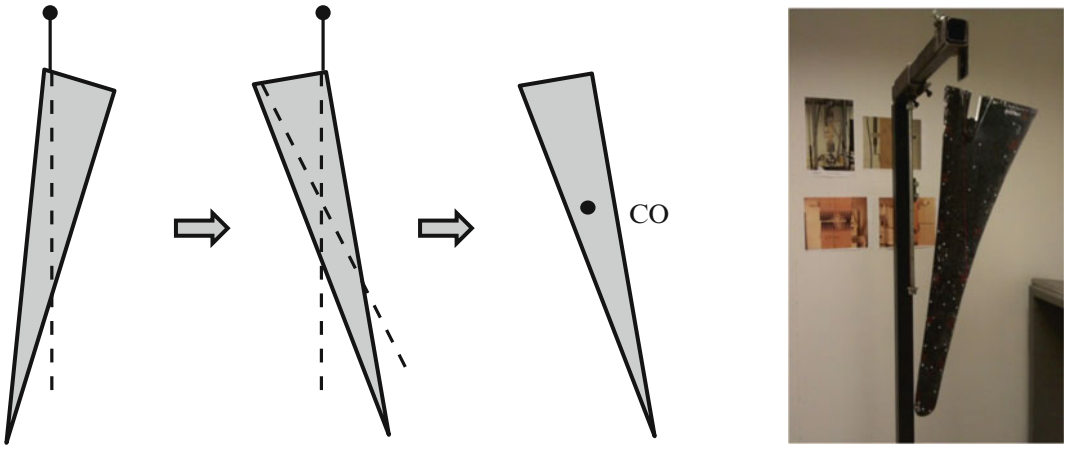

Fig. 21.10 (*Left*) Schematically-determination of the center of gravity by hanging the blade. (*Right*) Hanging the blade, vertical laser line in *red* (color figure online)

21.4.4 Blade Twist Angles

It is visible to the naked eye that the twisting, especially at the tips, differs from one blade to another. The twist of a blade affects the blade stiffness properties; a flat blade has a much larger moment of inertia in one direction than in the other and, therefore, resulting in a flexible and a stiff direction. When twisted, the stiffness increases in the weak direction and vice versa. This will lead to a coupling between the weak and the strong axis of the blade.

To gain knowledge about this, the twist of each blade is analyzed for three positions along the blades' x-axis. The spread is assumed to be due to the production process.

Some of the positions used for the vibrational tests are used to define the twist angles. To achieve this, a middle line between the opposing surface points is constructed for three selected intersections, see Fig. 21.2. It can be seen that the angles differ more and more towards the tip of the blade, which is as expected since the blade twist is cumulative. The maximum spread of angles is 11.91° (35.53° for blade D2 vs. 23.62° for blade B1). This spread is expected to give a noticeable variation of the blades' dynamical behavior. Figure 21.12 collects the angles for the three positions. There is nothing indicating that the blades are associated in sets based on similarity of angles which was verified by ANOVA in [9], although there seems to be a difference between measurements at Chalmers (A–D) and those at the Linnaeus University (E–G). This has not been investigated further.

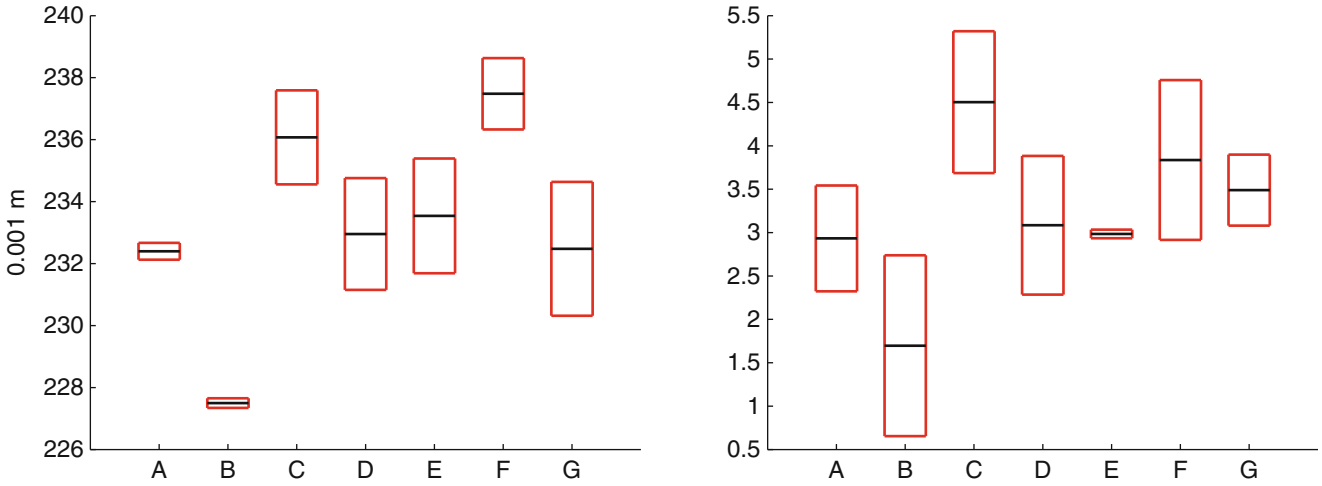

Fig. 21.11 Spread in the x- (*left picture*) and y-coordinate (*right picture*) of COG. Plus and minus one standard deviation, setting out from the black mean values, are represented by *red boxes* (color figure online)

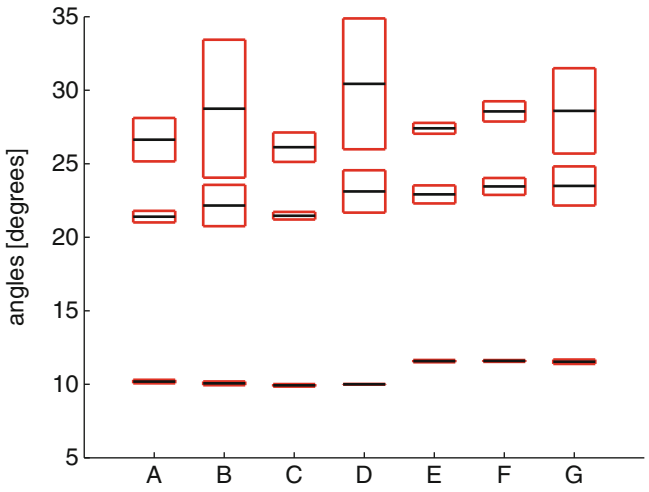

Fig. 21.12 Statistics for the twist angles. For each blade group (the columns), the mean value of the angle at each position is represented by a *black line*. Plus and minus one standard deviation, setting out from the mean values, are represented by *red boxes* (color figure online)

21.5 Conclusions

In this paper, a study of 20 blades for the Ampair 600 wind turbine, used as a benchmark structure by the SEM substructuring focus group, has been described. The study's aim is propagating manufacturing uncertainties backwards to the parameters of a Finite Element model.

Because of an over-parameterization of the glass fiber reinforced skin layer of the model, the spread in model parameters became higher than anticipated. Looking at the equivalent orthotropic material property however, the spread was a lot smaller. Static measurements of the skin tensile strength in the principal directions of the glass fiber weave indicated that the stiffness should be higher, but previous studies of material which has gone through the manufacturing process of the blades indicates that the results are reasonable.

The core properties were also undershooting the static coupon test results. By X-ray studies of core material in a blade, it was however found that the actual core has a much higher porosity than the coupon samples, which somewhat validates the results for the core stiffness as well.

ANOVA of measurements of the center of gravity of 19 blades indicates that the blades are balanced together in sets of three before being sent to customers.

There is a big spread in twist angles between blades within the same sets. This leads to differences in the dynamic behavior of the blades, even in sets that are grouped to work together. The mass, however, is quite equal within each set of blades. It can be concluded that the additional weights were definitely introduced to reach equilibrium of masses in each set.

While the proposed methodology for quantification of model parameter uncertainty has been shown to be of interest, the parameterization of the model is not as good as it could have been. The next step will be to include geometrical parameters such as blade twist into the calibration procedure.

A.1 Appendix

Table A.1 Eigenfrequencies (Hz) of the blades

Set	A					B				
Blade	828	852	790	μ	σ	841	722	819	μ	σ
Mode 1	45.6	46.5	48.4	46.9	1.45	45.2	45.2	43.6	44.7	0.92
Mode 2	129.3	128.9	128.1	128.8	0.62	128.8	124.6	128.8	127.4	2.41
Mode 3	191.2	190.7	198.7	193.5	4.49	189.2	203.5	185.1	192.6	9.64
Mode 4	248.8	251.5	240.7	247.0	5.60	248.3	241.0	247.6	245.6	4.02
Mode 5	323.9	312.4	317.9	318.1	5.71	320.5	331.1	311.7	321.1	9.72
Mode 6	399.1	386.8	394.6	393.5	6.25	391.8	387.6	393.7	391.0	3.14
Mode 7	427.3	411.4	406.5	415.1	10.90	406.5	412.1	437.8	418.8	16.67
Mode 8	467.7	435.1	464.8	455.9	18.03	462.1	471.2	454.9	462.8	8.19
Set	C					D				
Blade	878	877	881	μ	σ	963	962	948	μ	σ
Mode 1	46.7	47.6	45.3	46.5	1.16	46.4	44.3	46.9	45.9	1.35
Mode 2	128.2	134.1	126.9	129.7	3.84	129.6	124.4	130.3	128.1	3.19
Mode 3	191.3	192.3	200.0	194.5	4.72	191.9	193.6	198.5	194.6	3.42
Mode 4	245.7	255.4	244.1	248.4	6.16	251.0	241.2	249.2	247.1	5.20
Mode 5	315.3	315.1	328.5	319.6	7.66	323.6	330.2	324.2	326.0	3.67
Mode 6	390.1	401.6	393.3	395.0	5.93	398.8	385.4	389.6	391.3	6.82
Mode 7	400.5	413.0	443.4	419.0	22.06	404.4	404.7	405.5	404.8	0.56
Mode 8	469.4	466.9	464.0	466.8	2.73	478.6	482.5	478.5	479.9	2.30

	A–D		
	μ	σ	COV
Mode 1	46.0	1.37	0.03
Mode 2	128.5	2.55	0.02
Mode 3	193.8	5.24	0.03
Mode 4	247.0	4.63	0.02
Mode 5	321.2	6.78	0.02
Mode 6	392.7	5.17	0.01
Mode 7	414.4	14.0	0.03
Mode 8	466.3	12.5	0.03

Set	E				F				
Blade	905	912	μ	σ	893	906	907	μ	σ
Mode 1	43.40	42.28	42.84	0.56	46.27	42.25	46.78	45.10	2.03
Mode 2	122.56	119.51	121.04	1.53	125.73	121.51	128.07	125.11	2.71
Mode 3	169.96	171.78	170.87	0.91	181.27	175.51	184.08	180.29	3.57
Mode 4	237.44	233.30	235.37	2.07	244.40	237.37	247.94	243.24	4.39
Mode 5	298.77	297.39	298.08	0.69	305.36	301.74	307.05	304.71	2.22
Mode 6	380.93	369.33	375.13	5.80	390.78	378.30	396.58	388.56	7.63
Mode 7	438.42	442.16	440.29	1.87	452.04	449.16	459.99	453.73	4.58
Mode 8	533.94	530.42	532.18	1.76	548.90	536.98	553.22	546.37	6.86

Set	G					E–G		
Blade	888	892	895	μ	σ	μ	σ	COV
Mode 1	42.50	43.78	43.20	43.16	0.53	43.81	1.77	0.04
Mode 2	120.65	124.19	119.51	121.45	1.99	122.72	3.08	0.03
Mode 3	166.52	169.41	170.14	168.69	1.57	173.58	6.19	0.04
Mode 4	239.06	238.65	234.85	237.52	1.89	239.13	4.84	0.02
Mode 5	289.14	291.73	291.29	290.72	1.13	297.81	6.69	0.02
Mode 6	371.40	377.96	376.99	375.45	2.89	380.28	9.22	0.02
Mode 7	432.25	433.65	429.77	431.89	1.60	442.18	10.71	0.02
Mode 8	528.09	531.52	525.03	528.21	2.65	536.01	10.02	0.02

Set	A–G		
Blade	μ	σ	COV
Mode 1	45.1	1.85	0.04
Mode 2	126.2	3.96	0.03
Mode 3	185.7	11.56	0.06
Mode 4	243.9	6.07	0.02
Mode 5	311.8	13.47	0.04
Mode 6	387.7	9.26	0.02
Mode 7	425.5	18.73	0.04
Mode 8	494.2	36.81	0.07

Following, mean value (μ, Hz), standard deviation (σ, Hz) and coefficient of variation (COV, %) for each mode and all blades. The data for sets A–D are found in [9] and the data for sets E–G are found in [10]
Blades 893 and 907 show the greatest variation, with their frequencies being noticeably higher than that of the rest of the blades

Table A.2 Position of the center of gravity (mm) of the blades and masses (g)

Set	Blade	x	y	Mass
A	A1	232.23	3.55	818.8
	A2	232.25	2.33	816.6
	A3	232.71	2.92	818.2
	μ	232.40	2.93	817.9
	σ	0.27	0.61	1.14
B	B1	227.41	2.66	829.6
	B2	227.41	0.59	829.0
	B3	227.68	1.84	829.5
	μ	227.50	1.70	829.4
	σ	0.16	1.04	0.32
C	C1	236.62	4.96	812.1
	C2	237.24	4.99	812.4
	C3	234.36	3.56	812.7
	μ	236.07	4.50	812.4
	σ	1.52	0.82	0.30
D	D1	*	*	798.4
	D2	231.68	2.52	798.5
	D3	234.23	3.65	798.4
	μ	232.95	3.08	798.4
	σ	1.80	0.80	0.06
A–D	μ	232.17	3.05	814.5
	σ	3.47	1.29	11.63

* means that the center of gravity was not measured
Also, mean value (μ), and standard deviation (σ) for these variables

Set	Blade	x	y	Mass
E	E1	232.23	2.95	798.4
	E2	234.85	3.02	795.0
	μ	233.54	2.99	796.7
	σ	1.31	0.03	1.7
F	F1	238.80	3.64	812.3
	F2	236.95	3.03	812.0
	F3	236.69	4.84	814.4
	μ	237.48	3.84	812.9
	σ	0.94	0.75	1.1
G	G1	232.41	3.59	795.0
	G2	234.67	3.84	795.7
	G3	230.35	3.04	795.1
	μ	232.48	3.49	795.3
	σ	1.76	0.33	0.3
E–G	μ	234.62	3.52	802.2
	σ	2.83	0.69	8.9
A–G	μ	233.20	3.25	809.6
	σ	3.37	1.08	12.1

Also, mean value (μ), and standard deviation (σ) for these variables

Table A.3 Twist angles, at three locations along the blades, together with the mean values (μ), standard deviations (σ) and coefficients of variation (COV, %) for these

Set	A					B				
Blade	828	852	790	μ	σ	841	722	819	μ	σ
Angle 1	10.09	10.32	10.15	10.19	0.12	10.06	9.94	10.19	10.06	0.12
Angle 2	21.83	21.31	21.06	21.40	0.39	20.56	22.70	23.21	22.16	1.41
Angle 3	27.79	24.97	27.15	26.64	1.48	23.62	29.78	32.83	28.74	4.69
Set	C					D				
Blade	878	877	881	μ	σ	963	962	948	μ	σ
Angle 1	9.99	9.97	9.83	9.93	0.09	10.02	10.00	9.98	10.00	0.02
Angle 2	21.28	21.35	21.76	21.46	0.26	22.20	24.78	22.37	23.12	1.44
Angle 3	25.51	25.59	27.28	26.13	1.00	28.43	35.53	27.34	30.43	4.45

	A–D		
	μ	σ	COV
Angle 1	10.05	0.13	0.01
Angle 2	22.03	1.14	0.05
Angle 3	27.99	3.38	0.12

Set	E				F				
Blade	905	912	μ	σ	893	906	907	μ	σ
Angle 1	11.63	11.52	11.58	0.06	11.52	11.64	11.60	11.59	0.05
Angle 4	22.48	23.35	22.92	0.44	23.08	23.17	24.12	23.46	0.47
Angle 8	27.15	27.67	27.41	0.26	27.92	28.47	29.29	28.56	0.56

Set	G					E–G		
Blade	888	892	895	μ	σ	μ	σ	COV
Angle 1	11.37	11.66	11.57	11.53	0.12	11.56	0.09	0.01
Angle 4	22.00	24.56	23.91	23.49	1.09	23.33	0.85	0.04
Angle 8	25.36	29.45	30.97	28.59	2.37	28.28	1.69	0.06

	A–G		
Set	μ	σ	COV
Angle 1	10.65	0.77	0.07
Angle 4	22.55	1.20	0.05
Angle 8	28.11	2.77	0.10

References

1. Hemez F, Doebling S (2001) Model validation and Uncertainty Quantification. In: Conference Proceedings of the Society for Experimental Mechanics. 19th IMAC, 5–8 February, 2001, Kissimmee, FL
2. Khodaparast H, Mottershead J, Friswell M (2008) Perturbation methods for the estimation of parameter variability in stochastic model updating. Mech Syst Signal Process 22:1751–1773
3. Cheung SH, Beck J (2009) Bayesian model updating using hybrid Monte carol simulation with application to structural dynamic models with many uncertain parameters. J Eng Mech 135:243–255
4. Mayes RL (2012) An introduction to the SEM substructures focus group test bed - the Ampair 600 wind turbine. Conference Proceedings of the Society for Experimental Mechanics Series. 30th IMAC, A Conference on structural dynamics, 30 January–2 February, 2012, Jacksonville, FL
5. Rohe DP, Mayes RL (2013) Coupling of a bladed hub to the tower of the Ampair 600 wind turbine using the transmission simulator method. Conference Proceedings of the Society for Experimental Mechanics Series. 31st IMAC, A Conference on structural dynamics, 11–14 February, 2013, Garden Grove, CA
6. Rahimi S, de Klerk D, Rixen DJ (2013) The Ampair 600 wind turbine benchmark: results from the frequency based substructuring applied to the rotor assembly. Conference Proceedings of the Society for Experimental Mechanics Series. 31st IMAC, A conference on structural dynamics, 11–14 February, 2013, Garden Grove, CA
7. Macknelly D, Nurbhai M, Monk N (2013) Additional modal testing of turbine blades and the application of transmission simulator substructuring methodology for coupling. Conference Proceedings of the Society for Experimental Mechanics Series. 31st IMAC, A conference on structural dynamics, 11–14 February, 2013, Garden Grove, CA
8. Ampair Energy Ltd (2012) Ampair wind, hydro and packaged power specialists. Available at: http://www.ampair.com/wind-turbines/ampair-600. Accessed on 13, March, 2013
9. Gibanica M et al. (2013) Spread in modal data obtained from a wind turbine blade testing, Conference Proceedings of the Society for Experimental Mechanics Series. 30th IMAC, A conference on structural dynamics, 30 January–2 February, 2012, Jacksonville, FL
10. Kleinknecht M, Fernández Álvarez A (2013) Wind turbine blade modeling – setting out from experimental data, M.Sc. thesis, Linnaeus University
11. Harvie J, Avitabile P (2012) Comparison of some wind turbine blade tests in various configurations. Conference Proceedings of the Society for Experimental Mechanics Series. 30th IMAC, A conference on structural dynamics, 30 January–2 February, 2012, Jacksonville, FL, pp. 73–79
12. Johansson AT, Lindholm C-J, Khorsand M, Abrahamsson T (2013) Modeling and calibration of small-scale wind turbine blade, Conference Proceedings of the Society for Experimental Mechanics Series. 31st IMAC, A conference on structural dynamics, 11–14 February, 2013, Garden Grove, CA
13. Nimitiyongskul S, Kammer D (2009) Frequency band averaging of spectral densities for updating finite element models. J Vib Acoust 131:041007
14. Marquardt D (1963) An algorithm for least-squares estimation of nonlinear parameters. J Soc Indust Appl Math 11:431–441
15. Santner T, Williams B, Notz W (2003) The design and analysis of computer experiments. Springer, New York, NY
16. McKelvey T, Akcay H, Ljung L (1996) Subspace-based multivariable system identification from frequency response data. IEEE Trans Autom Control 41:960–979
17. Ljung L (1999) System identification: theory for the user, 2nd edn. Prentice Hall, Englewood Cliffs, NJ
18. Abrahamsson T, Kammer D (2014) FEM calibration with FRF damping equalization. In: Conference Proceedings of the Society for Experimental Mechanics Series. 32nd IMAC, A conference on structural dynamics, Orlando, FL
19. Martienssen W, Warlimont H (eds) (2005) Condensed matter and material data. Springer, Berlin